

Test Method

Shape optimisation of a biaxially loaded cruciform specimen

A. Makris^{a,*}, T. Vandenberg^a, C. Ramault^a, D. Van Hemelrijck^a, E. Lamkanfi^b,
W. Van Paepgem^b

^a Department of Mechanics of Materials and Constructions, Vrije Universiteit Brussel, Pleinlaan 2, 1050 Brussels, Belgium

^b Department of Materials Science and Engineering, Ghent University, 9000 Ghent, Belgium

ARTICLE INFO

Article history:

Received 31 August 2009

Accepted 8 November 2009

Keywords:

Cruciform type specimen

Biaxial loading

Finite element model (FEM)

Sequential quadratic optimisation (SQP)

ABSTRACT

In the present study, the shape of a cruciform type specimen under biaxial loading conditions is optimised. The basic goal is to achieve uniform biaxial failure in the centre of the specimen and minimise undesirable phenomena, such as premature failure outside the area of interest and non uniformities on the central strain field, caused by stress concentrations. A numerical optimisation technique (sequential quadratic programming or SQP) is coupled with a parametrically built finite element model (FEM) to concentrate and initiate damage in the centre and achieve a uniform strain field by varying the geometrical characteristics of the specimen. The outputs of the optimisation process are compared with a commonly used cruciform type geometry.

© 2009 Elsevier Ltd. All rights reserved.

1. Introduction

During their life time structures are often subjected to multiaxial loading conditions which can cause complex stress states, e.g. the internal pressure applied in a pressure vessel can lead to a biaxial or triaxial stress state on the walls of the vessel. Biaxial testing is an experimental technique which allows the investigation of the mechanical behaviour of materials under complex quasi-static or fatigue loading conditions. Over the years different techniques and specimens have been proposed to produce and investigate biaxial stress states [1,2], mostly for metallic or composite materials. These techniques may be classified into two general categories [3]: (i) tests using a single loading system and (ii) tests using two or more independent loading systems. In the first category the biaxial stress ratio depends on the specimen geometry or the loading fixture configuration; whereas in the second category it is specified by the applied load magnitude ratios. A versatile technique, representative of the second category, consists

of applying in-plane loads along two perpendicular arms of cruciform specimens [4–14]. In order to perform biaxial tests using this last kind of specimen, several biaxial testing devices have been proposed [15–20].

Multiaxial testing is of great interest for the investigation of the failure behaviour of composite materials. Their nonhomogeneous and strong anisotropic response, and the fact that such complex experiments demand expensive and sophisticated test equipment, can certainly justify why these kind of test methods have not obtained the same level of maturity as uniaxial testing. Moreover, this can possibly explain the small capability available to evaluate the multiaxial response of composite materials and to validate existing failure theories. The practice of using uniaxial test results to predict failure under multiaxial stress states seems inadequate [21,22].

A crucial issue for a successful biaxial test is the design of the specimen itself. An optimised cruciform specimen proper for biaxial testing should fulfil the following requirements: (i) maximisation of the region of strain uniformity in the biaxially loaded zone, (ii) minimisation of the global shear strains in the biaxially loaded test zone, (iii) minimisation of the strain concentrations/failure outside the test zone of interest, (iv) specimen failure in the

* Corresponding author. Tel.: +32 (0)2 629 29 36; fax: +32 (0)2 629 29 35.

E-mail address: andreas.makris@vub.ac.be (A. Makris).

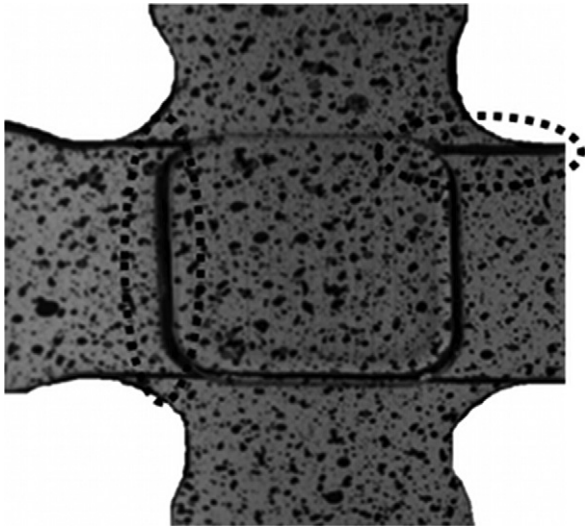


Fig. 1. Damaged areas of the cruciform specimen under 90% of the total failure load according to Digital Image Correlation Technique images.

biaxially loaded test zone and (v) repeatable results [7, 23–25]. It has been proven difficult to develop cruciform specimens that simultaneously fulfil all these requirements, therefore, in this study a numerical tool is developed and proposed to optimise the shape of the cruciform specimen with a focus on carbon epoxy cruciform specimens with a cross ply lay up. The specific material and lay up was selected because of the availability of numerical calculations and experimental data, for comparison and validation, while the developed method can be used for different kinds of materials and lay ups by applying small modifications in the code.

Previous studies considering failure analysis (using Digital Image Correlation Technique (DICT) and a Finite Element Damage Model (FEDM)) of carbon epoxy cross ply specimens [26], tested by using a commonly used cruciform geometry [4], pointed out problems such as strain concentrations and premature undesirable damage outside the area of interest, as illustrated in Figs. 1 and 3. These phenomena lead to a decrease in the accuracy of the obtained failure data. This study tries to bypass these problems by providing proper geometry modifications.

2. Numerical simulation of the biaxial test using shell elements

In order to simulate the mechanical test, a finite element model of the cruciform geometry was built using the commercial software Ansys[®]. In order to obtain the elastic properties and strength of the UD material, mechanical

tests were realized. Average five specimens per property were tested using on average five specimens per property. For the uniaxial tensile properties ISO-527-5 coupons were used, for the uniaxial compression properties ISO-14126 and all shear properties were measured by using the Iosipescu method (ASTM D5379). For generating through-thickness (TT) data in both tension and compression the circular-waisted block (CWB) [27] testing method was used. In Table 1 the average values and standard deviation of the elastic properties of the UD SE84 material can be found. These properties together with the strength of the lamina, see Table 2, were used as basic input for the FEM.

In Table 1, '123' is the fibre coordinate system, '1' is the fibre direction, '2' is the direction transverse to the fibres and '3' is the through-thickness direction (see Fig. 2).

In Table 2, X_T , X_C are the tensile and compressive strengths (expressed as stresses and strains) longitudinal to the fibres. Y_T , Y_C are the tensile and compressive strengths transverse to the fibres and normal to the '13' plane. Z_T , Z_C are the tensile and compressive strengths transverse to the fibres and normal to the '12' plane. S_{ij} ($i, j = 1, 2, 3$) is the shear strength of the lamina along the different axes.

To validate the FEM results, strain distribution data of the model are straightforwardly compared with experimental full field strain measurements obtained by using a Digital Image Correlation Technique (DICT). Fig. 3 shows the experimental and numerical strain results of a cruciform specimen under biaxial loading conditions where the load in the x-direction (horizontal) is 3 times that in the y-direction.

Comparison of the strain contour results confirms the good agreement between strain measurements and numerical predictions, validating the use of the numerical model for the optimisation process. The strain concentrations outside the zone of interest (i.e. outside the central biaxially loaded region), measured by the DICT and calculated by the FEM, emphasize the need for an improved shape that can fulfil the predefined requirements for a successful biaxial test.

3. Optimisation parameters and objective functions

Two different optimisation problems are solved: the first optimises a specimen with constant arm width (specimen (A)) which resembles the one found in [4,5] while the second optimises a specimen with a spline corner fillet (specimen (B)) [28]. These two specimen types are reported from the corresponding authors as the most promising among literature in producing accurate biaxial data and are plotted respectively left and right in Fig. 4 (above).

For both cases, the influence of six different geometrical parameters on the failure behaviour of the specimen was investigated (Fig. 4 (below)). For specimen A, the width and

Table 1
Elastic properties of the UD SE84 carbon lamina.

	E_1 [GPa]	E_2 [GPa]	E_3 [GPa]	G_{12} [GPa]	G_{23} [GPa]	G_{13} [GPa]	ν_{12}	ν_{23}	ν_{13}
Average	124.3	8.14	7.8	4.49	2.44	3.93	0.32	0.505	0.34
Standard deviation	4.4	0.1	0.12	0.07	0.21	0.1	0.02	0.005	0.025

Table 2
Strength of the UD SE84 carbon lamina expressed in stress (MPa) and strain (%) terms.

	X_T	X_C	Y_T	Y_C	Z_T	Z_C	S_{12}	S_{23}	S_{13}
Average [MPa]	2751	1180	25	162	42	165	106.9	35.21	97.87
Average [%]	2.14	1.21	0.46	2.41	0.46	2.41	2.8	1.1	2.8

the length of the specimen, the radius of curvature of the corner (f), the distance of the corner of the central section to the corner of the specimen (c), the number of layers of the central section (NLC) and the number of layers of the arm section (NLA) were varied. For specimen B, the central section becomes totally circular replacing parameter (c) (the corner distance) by the radius of the central circle (r), and parameter f (the curvature) by the position of the central point 'c' of the spline curve.

Each cruciform specimen is divided into two sections: the central part (section A), where the failure must be concentrated and, therefore, can be of reduced thickness, and the rest of the specimen including basically the arms (section B). A successful biaxial test is considered to be achieved by homogenous failure in section A. Hence, during the post analysis of each iteration the value of the Maximum Strain failure criterion (i.e. the percentage of the allowable strain reached) is stored for all the elements and layers. The maximal value of section B ($\xi_{\max,B}$) and the maximum value coming from the centre of section A ($\xi_{\max,A}$) are compared and divided, yielding a first objective function (the failure ratio, symbolized FR) reflecting the failure reached in both sections.

$$FR = \frac{\xi_{\max,B}}{\xi_{\max,A}} \quad (1)$$

The minimisation of this object function can lead to an optimised shape concerning damage initiation-concentration in the centre of the coupon. Moreover, a value smaller than 1 corresponds to a more evaluated failure in section A than in section B.

Another important characteristic for successful biaxial testing is the uniformity of the strain distribution in the biaxially loaded zone. For successful material testing, it should be as uniform as possible. In order to calculate the uniformity of the strain field, the strain data of the section A are used. The first principal strain values of all the central nodes are stored and the Coefficient of Variation (COF) of the sample is calculated. This COF represents the heterogeneity of the strain field and should, therefore, also be minimised.

$$COF = \frac{sd(\varepsilon_{\text{field}})}{\text{mean}(\varepsilon_{\text{field}})} \quad (2)$$

with $sd()$ and $\text{mean}()$ respectively, the standard deviation and the mean value of the strain field in section A.

Finally, a weighted sum of expression (1) and (2) leads to the 'multiobjective' cost function (CF) used in this study. The minimisation of this offers an optimum cruciform geometry considering concentration of the damage in the central section and uniformity of its strain distribution. Furthermore, it enables simultaneous consideration of both objective functions with a comparable scale:

$$CF = \frac{1}{wf \frac{FR_{\min,i}}{FR} + (1-wf) \frac{COF_{\min,i}}{COF}} \quad (3)$$

$|i = \text{specimenA} \vee \text{specimenB}$

In Eq. (3), $FR_{\min,i}$ and $COF_{\min,i}$ are the minimum values that can be found when optimising damage initiation or strain uniformity independently. A weight factor wf is used to tune the relative importance of the two objective functions (FR , COF) to the total one (CF). For this example, a factor $wf=0.8$ is used meaning that FR is 4 times more important than COF . The minimum theoretically attainable value of CF equals 1, corresponding to a specimen shape that optimises both FR and COF to their minimum value.

In order to ensure a manufacturable solution, the geometrical parameters are limited to the values given in Tables 3 and 4.

4. Optimisation process

The algorithm used for the optimisation is summarized in Fig. 5. The procedure starts by giving initial values to the geometrical parameters. A first step computes the stress and strain distribution in the specimen and automatically calculates the associated objective function. As long as the convergence criterion is not attained, the parameters are continuously updated by the optimisation algorithm. When two consecutive steps do not alter the objective function by more than 0.1%, convergence is assumed and the computation stops.

In this application, the selection of an appropriate optimisation algorithm is essentially dictated by the high computation time per iteration due to the FEA. It is, therefore, opted not to use global optimisation methods (e.g. genetic algorithm or simulated annealing) but local optimisation methods. Moreover, the convergence rate is increased by using algorithms based on higher order

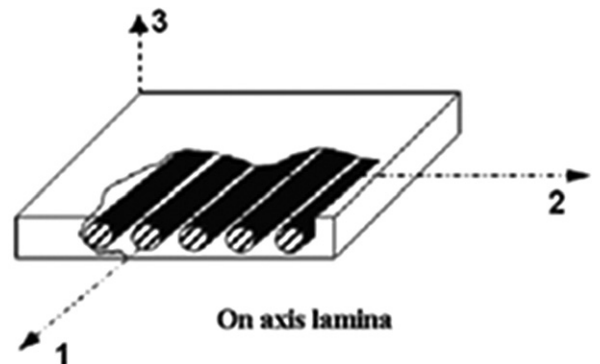


Fig. 2. Fibre coordinate system 123.

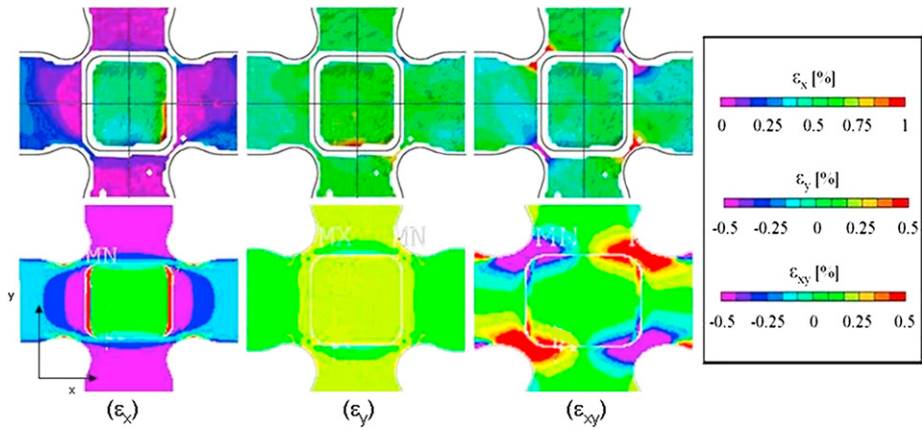


Fig. 3. ϵ_x , ϵ_y and ϵ_{xy} strain fields for a carbon epoxy cross ply cruciform specimen for 50% of the total failure load from DIC measurements (upper) and the finite element model (lower).

derivative information. Considering the type of optimisation problem (non-linear objective function with inequality constraints), Sequential Quadratic Programming (SQP) complies well with these fast convergence requirement. The method allows you to closely mimic Newton's method

for constrained optimisation just as is done for unconstrained optimisation. At each major iteration, an approximation is made of the Hessian of the Lagrangian function using a quasi-Newton updating method. This is then used to generate a Quadratic Programming (QP) sub-problem

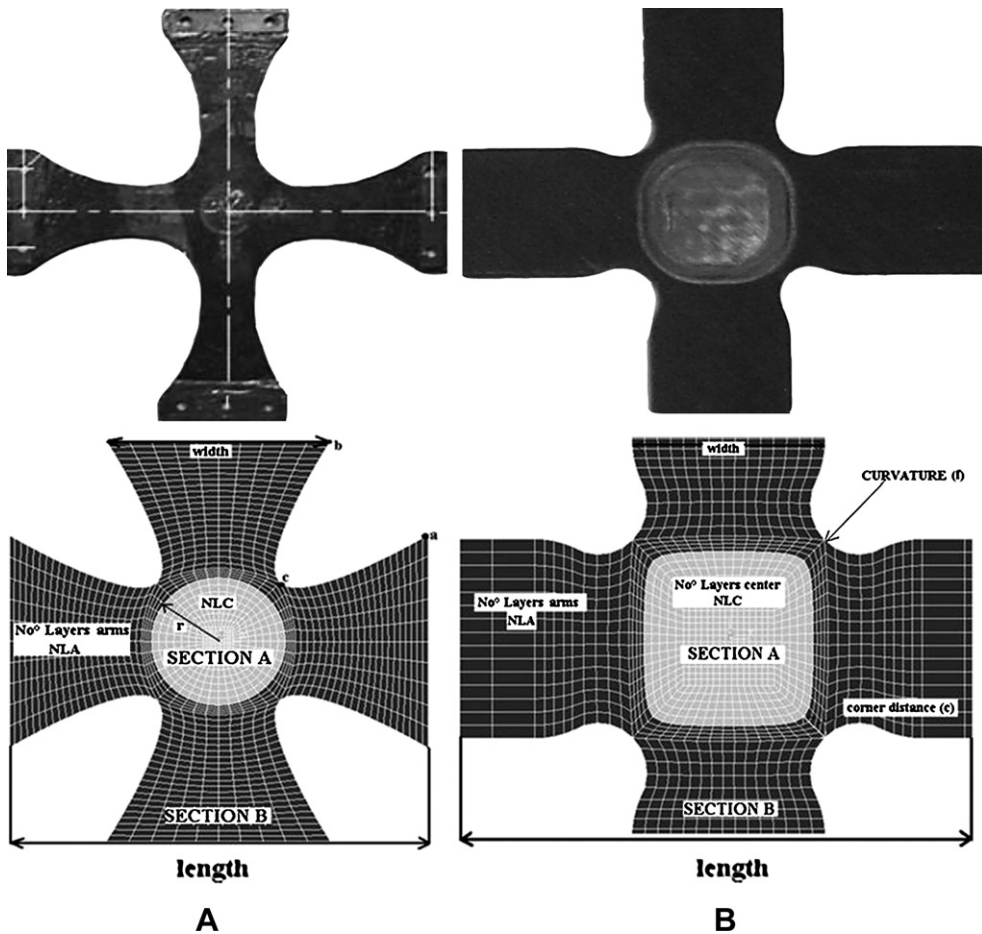


Fig. 4. Investigated geometrical parameters for the shape optimisation, for A) geometry with a fixed width, B) geometry with a spline corner fillet (through a, b and c points). Real specimen (above), simulation (below).

Table 3
Boundaries of the input parameters for specimen A.

Width (mm)	Length (mm)	f (mm)	c (mm)	NLA	NLC
20–80 with steps of 1 mm	150–300 with steps of 1 mm	4.2–24.9 steps of 0.1 mm	2 to width/2 with steps of 0.5 mm	4,8,12...40	4,8,12...20

Table 4
Boundaries of the input parameters for specimen B.

Width (mm)	Length (mm)	Radius (mm)	c (mm)	NLA	NLC
20–80 with steps of 1 mm	150–300 with steps of 1 mm	1–1.2*c with steps of 0.2 mm	20 to length/5 with steps of 0.2 mm	4,8,12...40	4,8,12...20

whose solution is used to form a search direction for a line search procedure. A detailed overview of SQP can be found in [29,30]. The general method, however, is stated in [31] and summarized here. The optimisation problem is formulated as follows:

$$\text{Minimise } f(\bar{x}) \quad \bar{x} \in \mathfrak{R}^n \tag{4}$$

$$\text{Subject to } h_i(\bar{x}) = 0 \quad i = 1, \dots, m$$

$$h_i(\bar{x}) \geq 0 \quad i = m + 1, \dots, r$$

Expression (4) is called the standard form [32] in which the function $f: \mathfrak{R}^n \rightarrow \mathfrak{R}$ is referred to as the objective function or cost function (here the strain uniformity, the failure ratio or finally a function of both) and in which the vector $\bar{x} = (x_1, \dots, x_n)$ is called the optimisation variable or

design vector of the problem (here the geometrical parameters of the specimen). The functions $h_i: \mathfrak{R}^n \rightarrow \mathfrak{R}$, $i = 1, \dots, m$ are the equality constraints and $h_i: \mathfrak{R}^n \rightarrow \mathfrak{R}$, $i = m + 1, \dots, r$ are the inequality constraints (above mentioned limits imposed for manufacturing).

The principal idea is the formulation of a QP sub-problem based on a quadratic approximation of the Lagrangian function

$$L(\bar{x}, \bar{\lambda}) = f(\bar{x}) + \sum_{i=1}^m \lambda_i h_i(\bar{x}) \tag{5}$$

The QP sub-problem is obtained by linearizing the non-linear constraints. This sub-problem can be solved using any QP algorithm (explained in [31,33]). The obtained QP sub-problem is of the following form

$$\text{Minimise } q(\bar{d}_k) = \frac{1}{2} \bar{d}_k^T H_k \bar{d}_k + \nabla f(\bar{x}_k)^T \bar{d}_k \quad \bar{d}_k \in \mathfrak{R}^n \tag{6}$$

$$\text{Subject to } \nabla h_i(\bar{x}_k)^T \bar{d}_k + h_i(\bar{x}_k) = 0 \quad i = 1, \dots, m$$

$$\nabla h_i(\bar{x}_k)^T \bar{d}_k + h_i(\bar{x}_k) \leq 0 \quad i = M + 1, \dots, r$$

with \bar{d}_k the search direction at iteration k and H_k the Hessian of the Lagrangian function L at iteration k . The two lower expressions in Eq. (6) represent the linearized constraints. If no analytical solution is available for the Hessian (as is the case here), it can be estimated by finite differences, but at the cost of high computation intensity. Therefore, the Hessian H of the Lagrangian function L is approximated by a positive definite matrix using the BFGS-method (Broyden-Fletcher-Goldfarb-Shanno)

$$B_{k+1} = B_k - \frac{B_k s_k s_k^T B_k}{s_k^T B_k s_k} + \frac{y_k y_k^T}{y_k^T s_k} \tag{7}$$

with $y_k = \nabla L_{k+1} - \nabla L_k$ and $s_k = x_{k+1} - x_k$. As a starting point, B_0 can be set to the identity matrix I . The solution of the QP

Table 5
Converged values of the cost function (CF) starting from different initial input values (geometries 1–5).

	1	2	3	4	5
CF: Specimen A	1.1152	1.0547	1.0442	1.0462	1.3962
CF: Specimen B	1.5535	1.1843	1.1843	1.2022	1.1882

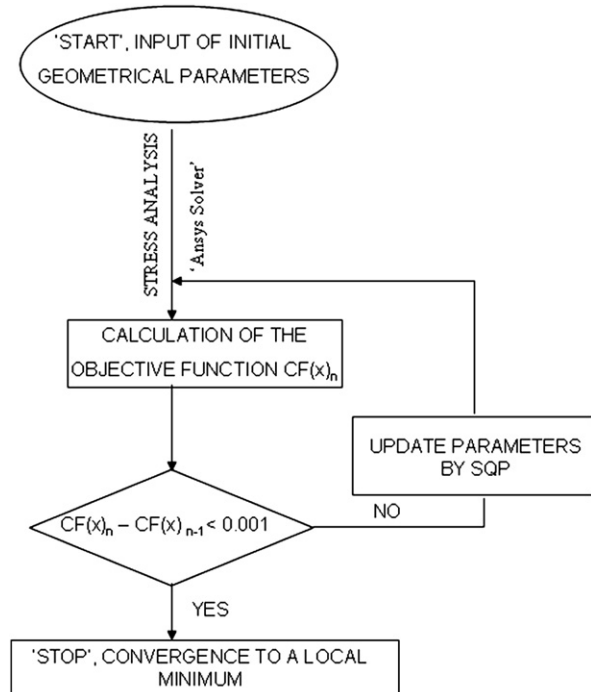


Fig. 5. Flowchart for the geometrical parameter updating.

Table 6

Minimum found objective functions for the optimised specimen A and B, and a commonly tested specimen.

	Optimal specimen A	Optimal specimen B	Commonly tested Geometry
FR	0.716	0.488	1.6982
COF	0.168	0.152	0.1850
CF	1.044	1.184	2.4746

sub-problem (6) is used as search direction \bar{d}_k for a new iteration

$$\bar{x}_{k+1} = \bar{x}_k + \alpha_k \bar{d}_k \tag{8}$$

The last step of the iteration consists of determining the step length parameter α_k in order to produce a sufficient decrease in a merit function. The merit function used by Han [34] and Powell [35] is used in this implementation

$$\Psi(\bar{x}) = f(\bar{x}) + \sum_{i=1}^m r_i \cdot h_i(\bar{x}) + \sum_{i=m+1}^r r_i \cdot \max\{0, h_i(\bar{x})\} \tag{9}$$

Table 7

Parameter values for the two optimised specimens.

	Width (mm)	Length (mm)	f/Radius (mm)	c (mm)	NLC	NLA
Specimen A	31	222	9.4	2	4	40
Specimen B	49	296	23.6	20	4	40
Commonly tested Geometry	25	250	6.25	3.76	8	16

with $r_i = r_{i, \text{iteration } k+1} = \max\{\lambda_i, 1/2(r_{i, \text{iteration } k} + \lambda_i)\}$ for $i = 1, \dots, m$ as recommended by Powell [35]. This allows positive contribution from constraints that are inactive in the QP-solution but were recently active. In this implementation, the penalty parameter r_i is initially set to

$$r_i = \frac{\|\nabla f(\bar{x})\|}{\|\nabla h_i(\bar{x})\|} \tag{10}$$

which ensures larger contributions to the penalty parameter from constraints with smaller gradients, which could be the case for active constraints at the solution point.

This SQP method is implemented as such in the Matlab[®] optimisation toolbox and detailed information can be

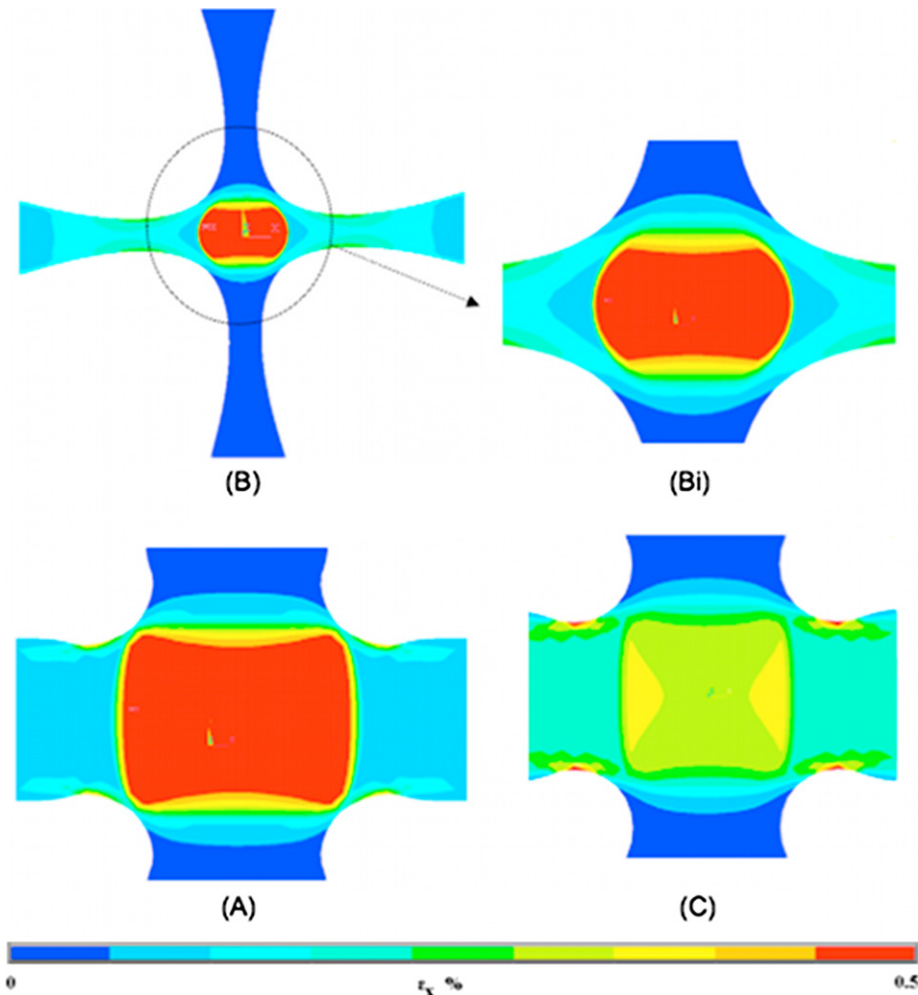


Fig. 6. Normal Strain ϵ_x distribution (0–0.5%) of the two optimised geometries B (Bi detail) and A, and for the commonly tested case (C).

found in [31]. This method allows fast convergence towards a feasible local minimum but does not necessarily guarantee to end in the global minimum. Therefore, the optimisation algorithm is started from different initial points (i.e. input values that correspond to different initial specimen geometries). Table 5 gives an example of the obtained objective function (*CF*), starting from five different specimen geometries. The fact that the results are showing convergence towards the same minimum indicates the high possibility that the global minimum is found.

5. Results and discussion

The optimisation of the geometry was performed for the equibiaxial loading case (load ratio 1/1) and by using the total cost function (*CF*). The significant decrease in the objective function (*FR*) (57.8% for specimen A and 71.2% for specimen B) in comparison with the commonly used tested geometry, demonstrates an important increase in damage initiation inside section A. An improvement in the central strain distribution is also achieved when comparing the *COF* values (9.2% for specimen A and 17.8% for specimen B). Furthermore, when comparing the two optimum geometries found, for the two individual objective functions (*FR* and *COF*), specimen B represents a better solution, as it achieves a lower failure ratio (*FR*) and uniformity value (*COF*), see Table 6.

Table 7 lists the geometrical parameter values for both optimised solutions by using the (*CF*) objective function together with the values of the commonly tested geometry.

In order to better visualize the results, the output of the strain distribution in the *x*-direction (ϵ_x) is also presented in Fig. 6 for three cruciform geometries, the optimum specimens A, B and the commonly used tested geometry. For the two optimised geometries, the maximum strain value is calculated in the central section while for the third geometry on the corners of the specimen, proving that an improvement has been achieved.

6. Conclusions

A numerical optimisation methodology is proposed in order to achieve higher quality biaxial tests. By modifying the specimen's geometry, one can augment the strain uniformity in the biaxially stressed region and/or concentrate failure in this same region.

The optimisation procedure is based on the analysis of the specimen by a (shell) finite element model, while the geometry optimisation and updating is performed by Sequential Quadratic Programming.

Two different specimens were compared: a cruciform with constant arm width and one with a spline corner fillet. It is found that the latter enables to achieve higher damage concentration in the central section. Furthermore, both optimum solutions show higher strain uniformity in that region than the commonly tested geometry.

The user-friendly implementation allows tuning the relative importance accorded to damage initiation compared to strain uniformity. Moreover, it enables extension for further analysis, for example, shape

optimisation considering different materials, stacking sequences or objective functions.

References

- [1] A.S. Chen, F.L. Matthews, A review of multiaxial/biaxial loading tests for composite materials. *Composites* 24 (1993) 395–406.
- [2] A. Makris, C. Ramault, D. Van Hemelrijck, A. Clarke, C. Williamson, M. Gower, R. Shaw, R. Mera, E. Lamkanfi, W. Van Paepegem. A review of biaxial test methods for composites, in: *International Conference on Experimental Techniques*, 2007.
- [3] A. Zouani, T. Bui-Quoc, M. Bernard, A proposed device for biaxial tensile fatigue testing ASME PVP-323. *Fatigue and Fracture* 1 (1996) 331–339.
- [4] A. Smits, D. Van Hemelrijck, T.P. Philippidis, A. Cardon, Design of a cruciform specimen for biaxial testing of fibre reinforced composite laminates. *Composites Science and Technology* 66 (7–8) (2006) 964–975.
- [5] J.S. Welsh, D.F. Adams, An experimental investigation of the biaxial strength of IM6/3501-6 carbon epoxy cross ply laminates using cruciform specimens. *Composites Part A* 33 (2002) 829–839.
- [6] I.H. Wilson, J. White, Cruciform specimens for biaxial fatigue tests: an investigation using finite element analysis and photoelastic-coating techniques. *Journal of Strain Analysis* 6 (1971) 27–37.
- [7] H.J. Kwonz, Z. Xia, B. Jar, Characterization of biaxial fatigue resistance of polymer plates. *Journal of Materials Science* 40 (4) (2005) 965–972.
- [8] A.G. Atkins, G. Jeronimidis, S. Arndt, Biaxial monotonic and fatigue fracture of some commercial ABS and PVC sheets. *Journal of Materials Science* 33 (1998) 4349–4356.
- [9] C. Jones, Biaxial testing of polymer matrix composites. *Materials World* 9 (2001) 19–21.
- [10] K.J. Pascoe, P.A. Tutton, Biaxial testing of multi-laminate fiber composites, in: *Proceedings of the Third Riso International Symposium on Metallurgy and Materials Science*, 1982, pp. 265–270.
- [11] C.W. Bert, B.L. Mayberry, J.D. Ray, Behavior of Fiber Reinforced Plastic Laminates Under Biaxial Loading ASTM STP (1969).
- [12] D. Van Hemelrijck, C. Ramault, A. Makris, E. Lamkanfi, W. Van Paepegem, D. Lecompte, Biaxial testing of fibre reinforced composite laminates. *Proceedings of the Institution of Mechanical Engineers, Part L: Journal of Materials: Design and Applications* 222 (L4) (2008) 231–239.
- [13] E. Lamkanfi, W. Van Paepegem, J. Degrieck, C. Ramault, A. Makris, D. Van Hemelrijck, Strain distribution in cruciform specimens subjected to biaxial loading conditions. Part 1: two-dimensional versus three-dimensional finite element model, *Polymer Testing* (2009).
- [14] E. Lamkanfi, W. Van Paepegem, J. Degrieck, C. Ramault, A. Makris, D. Van Hemelrijck, Strain distribution in cruciform specimens subjected to biaxial loading conditions. Part 2: Influence of geometrical discontinuities (2009).
- [15] E. Shiratori, K. Ikegami, A new biaxial tensile testing machine with flat specimen. *Bulletin of the Tokyo Institute of Technology* 82 (1967) 105–118.
- [16] M.W. Parsons, K.J. Pascoe, Development of a biaxial fatigue testing rig. *Journal of Strain Analysis* 10 (1975) 1–9.
- [17] G. Ferron, A. Makinde, Design and development of a biaxial strength testing device. *Journal of Testing and Evaluation* 16 (1988) 253–256.
- [18] H. Fessler, J. Musson, A 30ton biaxial testing machine. *Journal of Strain Analysis* 4 (1969) 22–26.
- [19] A. Makinde, L. Thibodeau, K.W. Neale, Development of an apparatus for biaxial testing using cruciform specimens. *Experimental Mechanics* 32 (2) (1992) 138–144.
- [20] J.P. Boehler, S. Demmerle, S. Koss, A new direct biaxial testing machine for anisotropic materials. *Experimental Mechanics* 34 (1994) 1–9.
- [21] P.D. Soden, M.J. Hinton, A.S. Kaddour, Biaxial test results for strength and deformation of a range of E-glass and carbon fibre reinforced composite laminates: failure exercise benchmark data. *Composites Science and Technology* 62 (2002) 1489–1514.
- [22] J.S. Welsh, D.F. Adams, Development of an electromechanical triaxial test facility for composite materials. *Experimental Mechanics* 40 (3) (2000) 312–320.
- [23] M. Geiger, W. Hubn, M. Merklein, Specimen for a novel concept of the biaxial tension test. *Journal of Materials Processing Technology* 167 (2005) 177–183.
- [24] S. Demmerle, J.P. Boehler, Optimal design of biaxial tensile cruciform specimens. *Journal of the Mechanics and Physics of Solids* 41 (1993) 143–181.

- [25] Y. Yu, M. Wan, X.D. Wu, Design of a cruciform biaxial tensile specimen for limit strain analysis by FEM. *Journal of Materials Processing Technology* 123 (2002) 67–70.
- [26] A. Makris, D. Van Hemelrijck, C. Ramault, D. Zarouchas, E. Lamkanfi, W. Van Paepegem, An investigation of the mechanical behavior of carbon epoxy cross ply cruciform specimens under biaxial loading. *Polymer Composites* (2009).
- [27] W.R. Broughton, G.D. Sims, An Overview of Through-Thickness Test Methods for Polymer Matrix Composites NPL Report DMM (A) 148. National Physical Laboratory, Middlesex, UK, 1994.
- [28] E.H. Rochdi, D. Bigaud, E. Ferrier, P. Hamelin, Ultimate behaviour of CFRP strengthened RC flat slabs under a centrally applied load. *Composite Structures* 72 (2006) 69–78.
- [29] R. Fletcher, *Practical Methods for Optimisation*. John Wiley and Sons, Great Britain, 1987, p. 436.
- [30] A. Teughels, Inverse Modelling of Civil Engineering Structures Based on Operational Modal Data. Katholieke Universiteit Leuven, Belgium, 2003, p. 250.
- [31] *Optimisation Toolbox User's Guide* (5th Printing). MathWorks, United States of America, 2004, p. 204.
- [32] S. Boyd, L. Vandenberghe, *Convex Optimisation*, first ed. Cambridge University Press, UK, 2004, p. 730.
- [33] D. Lecompte, Elastic and Elasto-Plastic Material Parameter Identification by Inverse Modelling of Static Tests Using Digital Image Correlation. Vrije Universiteit Brussel and Koninklijke Militaire School, Belgium, 2007, p. 251.
- [34] S.P. Han, A globally convergent method for nonlinear programming. *Journal of Optimisation Theory and Applications* 22 (1977) 297.
- [35] M.J.D. Powell, A fast algorithm for nonlinearity constrained optimisation calculations. in: G.A. Watson (Ed.), *Numerical Analysis, Lecture Notes in Mathematics*, vol. 630. Springer Verlag, 1978.